Quantification of protective properties of the coating/corrosion product/steel interface by integration of transmission line model with EIS results

J. Niu, J. I. Barraza-Fierro, H. Castaneda

Abstract An experimental set up was designed to characterize and quantify the protective properties of coated steel samples over time. A porous layer of corrosion products (Fe_xO_y) was formed on the metal surface prior to coating application to simulate the coating disbondment condition. The detailed sample system configuration is as follows: coal tar epoxy coating/corrosion product/steel substrate. A continuous damage evolution mechanism was proposed which contains the following three stages: (I) mass transport within the coating and the corrosion porous layer, (II) mass transport and charge transfer mechanism mixture due to the formation of active sites beneath the coating layer, and (III) charge transfer dominant mechanism due to adsorption and electrochemical reaction. This damage evolution concept was supported by the experimental results in this work. Based on the electrochemical impedance spectroscopy (EIS) technique, we observed that the sample system underwent stage I when initially immersed in an electrolyte solution. By evaluating the induced disbondment conditions, transitions from stage I to stages II and III were observed during the experimental period. After 55 days of exposure, stage III was identified in the EIS spectra. A transmission line model and EIS analysis was applied to each experimental condition. The simulated impedance magnitude has a good agreement with the experimental results.

Keywords Damage evolution, Coating disbondment, EIS, Transmission line model

J. Niu, J. I. Barraza-Fierro, H. Castaneda (✉)
Chemical and Biomolecular Engineering Department, NCERCAMP, The University of Akron, 264 Wolf Ledges Parkway, Akron, OH, USA
e-mail: homeroc@uakron.edu

Introduction

One classical method of corrosion control that is used to preserve metals from corrosive environments is to apply a physical barrier to the metallic substrate.[1,2] The objective is to protect the metallic substrate from corrosive environments and retard the transportation of corrosive species (i.e., water, ions, and oxygen) through the coating layer.[3] However, coatings and the coating/substrate interface can be chemically and mechanically degraded over time,[4,5] the former by the swelling process and the latter when the interface between the coating and the substrate deteriorates by delamination or disbondment.[4,6]

The general protective properties for the ''coating on steel'' system have been characterized using various different technologies and quantified using theoretical models. Different techniques and approaches are used to characterize the performance and degradation of the coating/steel system. For example, localized electrochemical impedance (LEIS) has been used to study the surface morphology during coating deterioration[7] and surface evolution during different stages of coating degradation. Additionally, electrochemical techniques include electrochemical noise (EN), which has been used to characterize the initial stage of coating damage,[8] and electrochemical impedance spectroscopy (EIS), which has been extensively applied to study the degradation of coating/metallic substrate materials by evaluating each element in the electrochemical cell.[9,10]

In general, EIS has been used to analyze and quantify the mechanistic processes occurring at each formed interface, e.g., coating/substrate and electrolyte/coating; and different data analysis approaches have been applied such as transfer function analysis and equivalent circuit elements. This latter approach has led to qualitative analysis of the deterioration of organic coatings[11] and the bonding between coatings

and metals under several exposure conditions. For example, Deflorian et al.[12] studied the effect of environmental factors, such as UV exposure, temperature, and humidity, whereas Akbarinezhad et al.[13] investigated the variation in coating resistance and capacitance during coating chemical degradation. In addition, Walter[14] studied the effects of water uptake and chloride ion concentration on the degradation of coating/metal systems and Haruyama et al.[15] analyzed the delamination ratio of coatings by determining the breaking point frequency.

Due to the extended testing periods that adequately characterize the damage stage, water uptake, electrochemical initiation at the coating/corrosion product/substrate interface, and coating delamination/substrate damage have been studied separately. Based on previous works,[10,16] continuous and parallel processes related to the initial degradation of coatings, such as electrolyte penetration (water uptake), have been extensively studied.[14,15]

This evolution damage for coating detachment can cover different stages from initial immersion of the sample to failure of the coating and substrate activation. The ions transported through the coating and the damage mechanism can be divided in the following three general stages: (1) the transportation of ions (mass transfer) from the aqueous environment within the coating layer and the preformed corrosion product layer[17]; (2) the mixed mechanisms of mass transfer and charge transfer due to the formation of active sites, and (3) the charge transfer[10,11] mechanism as the dominant processes during the metallic dissolution process.

In this article, the initial corrosion product layer was chemically created via precipitation of a porous oxide film between the coating and the steel. This condition simulates bad surface preparation conditions by creating an initial layer. This artificial coating disbondment was studied by means of EIS and the results were characterized through transmission line modeling (TLM). TLM quantifies a corrosion system by dividing an electrochemical interface into sub-elements of defined scale, which is compared to the entire system. For example, TLM was previously used to obtain the impedance distribution of pores in an iron oxide layer (hematite).[18] TLM has been used to characterize porous electrodes[19] and iron oxide layers with varying oxygen–iron ratios.[20] TLM was also widely used to study the evolution of magnesium-rich primer.[21,22] In this study, TLM was used to describe and quantify the influence of each layer: the porous iron oxide inner layer formed initially at the steel surface and the coating outer porous layer. Samples with two coating thicknesses were tested in a 3.5 wt% NaCl electrolyte solution with pH 4.0 for 55 days and characterized by TLM.

Experimental

Substrate

Carbon steel 1018 samples were used as the metallic substrate. The nominal chemical composition in wt% was $\leq 0.18\%$ C, 0.6–0.9% Mn, $\leq 0.04\%$ P, ≤ 0.04, and balance Fe.

Corrosion product formation on the metal substrate

The process of iron oxide formation that was used to prepare the substrates is called bluing or browning[23] and is described as follows. The 1018 carbon steel plates were immersed into a solution containing 1 kg L^{-1} NaOH and 0.3 kg L^{-1} KNO$_3$ for 10 min at 120°C followed by a washing process. This included immersion in an 80°C DI water bath for 30 min. A brownish layer was formed on the surface of the carbon steel and its thickness was measured with a coating thickness gage (Elcometer 456). The average thickness of the artificial oxide layer was 6 ± 0.1 μm. After the artificial oxide layer formed on the substrate, the samples were then coated with Targuard Coal Tar Epoxy©. The epoxy coating was directly applied on the sample substrate surface by conventional spray without any pretreatment. The samples were classified into two groups based on the coating thicknesses: 0.13 and 0.50 mm. The iron oxide layer formed on the steel surface simulated poor steel surface conditions and/or poor coating adherence referred to as artificial disbondment conditions.

Experimental set up

EIS measurements were performed in a three-electrode electrochemical cell. Metal/oxide/coating samples with a surface area of 4.52 cm^2 were used as the working electrode, a saturated calomel electrode (SCE) was used as the reference electrode, and a platinum mesh with a hole in the center served as the counter electrode.

The electrolyte was prepared with 3.5 wt% NaCl at pH 4.0. The pH was kept constant using buffer solutions (sodium acetate/acetic acid).[24,25]

Surface analysis

After the oxide formation, infinite focus microscopy (IFM) and X-ray photoelectron spectroscopy PHI VersaProbe XPS microprobe techniques were performed at the surface of the carbon steel samples.

Electrochemical impedance testing

A Gamry Reference 600[TM] was used to perform the EIS and open-circuit potential measurements. The EIS data were collected over a frequency range from 10 mHz to 20 kHz with a voltage amplitude of ±10 mV from the corrosion potential. The data acquisition was controlled by Gamry Framework Version 5.8/EIS 300 software. All the measurements were performed at room temperature.

Results and discussion

Composition and morphology analysis of the artificial oxide layer

X-ray photoelectron spectroscopy (XPS) results

The take-off angle in this measurement was zero, the source of XPS used was monochromatic (Al Kα) X-ray beam, and the data was processed with Multipak version 9.

A wide-scan XPS spectrum (Fig. 1) indicates that the main elements in the oxide layer are iron and oxygen, which can be represented as Fe_xO_y. According to the Pourbaix diagram,[26] the oxides Fe_2O_3 and Fe_3O_4 are the main products formed at medium and high pH and these oxides are detected after surface steel treatment processes such as bluing and browning.[23] The initial iron oxide product detected on the steel surface was Fe_3O_4. However, other ratios of iron and oxygen occurred (Fe_xO_y or Fe_mO_n). These ratios and their mechanical–physical properties depend on many factors, such as oxygen and iron concentration, pressure, temperature, electrolyte, and pH.[27] In our study, the stoichiometry of the iron oxide that was produced on the metallic surface was assumed to be represented as Fe_xO_y.

Infinite focus microscopy (IFM) results

The morphology of the oxide products and coating layers were characterized using optical microscopy. A
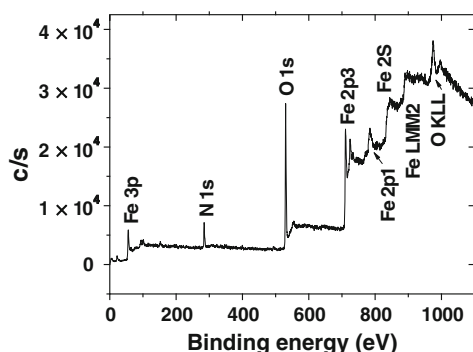

Fig. 1: Wide-scan XPS spectrum of the oxide film

top view of the experimental set up is shown in Fig. 2a; this contains a dashed square that is expanded in Fig. 2b. The purpose is to compare the degraded coating with the intact one of a plate immersed in a solution at pH 4 for 55 days. In Fig. 2b, the top right area is the coating that remained intact because it was not exposed to the electrolyte solution. The bottom left area in Fig. 2b is the region that was exposed to the pH 4 electrolyte solution. The valleys resulted from areas of damaged coating that were detached from the metal surface.

Damage of the interface at acid conditions

The concentration of ionic species in the aqueous solution influences coating and metal degradation processes. In this study, pH 4 electrolyte was evaluated with a buffer solution to control the pH at longer exposure times (55 days).

Figure 3a shows the Nyquist representation for a steel sample with a porous iron oxide inner layer (Fe_xO_y) and a coal tar epoxy outer layer that was exposed to a solution of 3.5 wt% NaCl at pH 4. On day 1, one loop was observed at high frequency (HF), and the initial part of a second loop was observed at low frequency (LF). The loop at HF is associated with the coating layer, as previously described by Mansfeld.[28] The diameter of the HF semicircle could be related to an inhomogeneous water/electrolyte distribution in the coating while the loop at LF is associated with the iron oxide/substrate interface and indicates the initiation of electrochemical reactions on the iron oxide surface and/or the metallic substrate.[29] On day 3, the coating/steel system is assumed to face stage II where two loops were observed. Compared to the first day, the semicircle at LF is better defined and larger than the one at HF. At 10 and 21, a semicircle at HF to medium frequency (MF) and a semipositive loop at LF, while at 31 and 55 days, a semicircle at HF to MF and a positive loop at LF were observed. This behavior could be related to a process mixture for coating resistance (due to mass transport) and electrochemical reactions (charge transfer). This latter could be at the substrate/oxide/electrolyte interface at 10 and 21 days, while the adsorption could be at the oxide pore wall and base at 31 and 55 days. On days 31 and 55, the adsorbed intermediate ionic species and the charge transfer resistance at the corrosion porous layer/substrate interface were the dominant mechanisms influencing electrochemical reactions.

Effect of the coating thickness

The effect of the coating thickness at pH 4 is shown in Figs. 3a and 3b for 0.13 mm and Figs. 4a and 4b for 0.50 mm thickness. The presence of two semicircles in Fig. 3a and their evolution with time was described in the previous section. Afterward, the total impedance
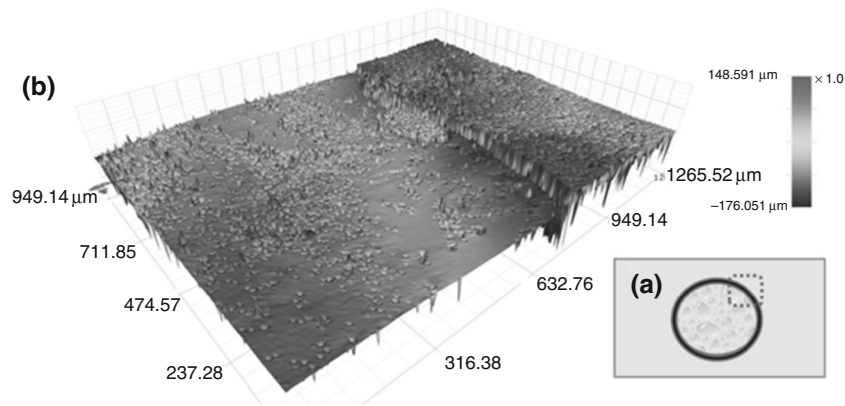
Fig. 2: **(a) Top view of the experiment set up and (b) the morphology of the edge of the electrochemical cell after being immersed in electrolyte solution at pH 4.0 for 55 days**
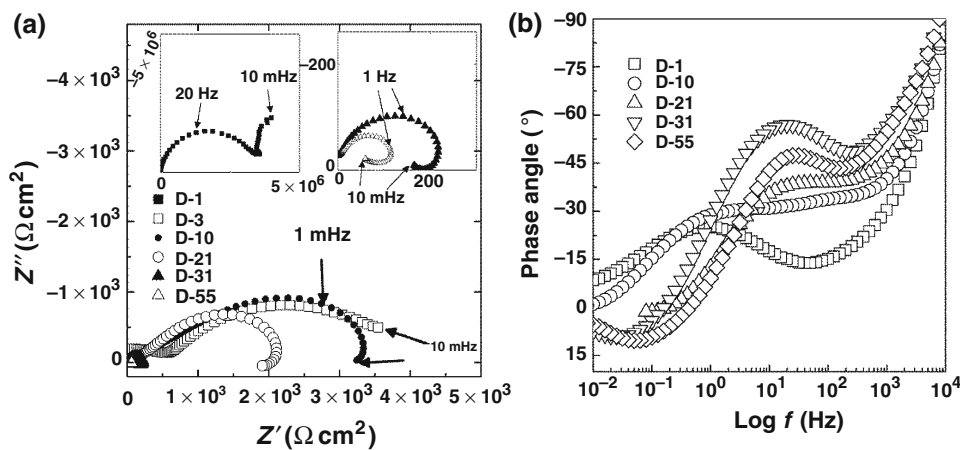

Fig. 3: **(a) Nyquist diagram; (b) Phase angle diagram of a plate coated with 0.13 mm of coal tar in NaCl solution at pH 4**
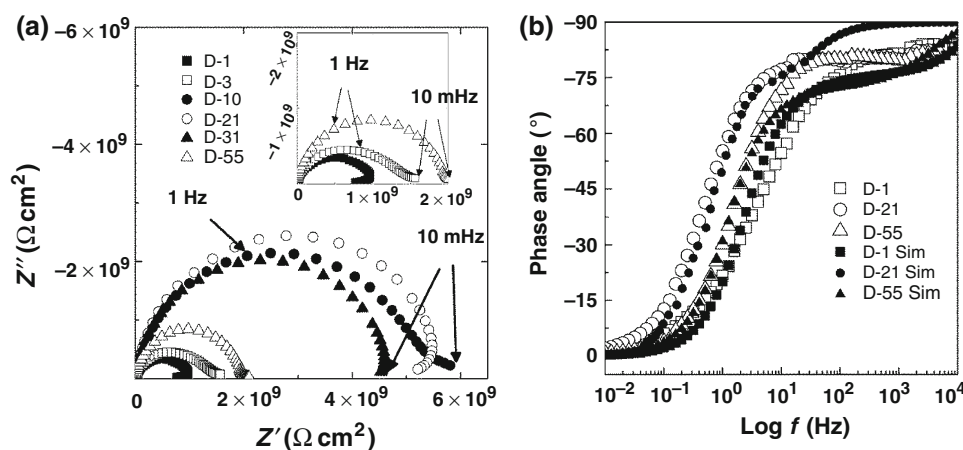

Fig. 4: **(a) Nyquist diagram; (b) Phase angle diagram of a plate coated with 0.5 mm of coal tar in NaCl solution at pH 4**

decreased due to the water uptake and/or a coating transformation. In the early period (10 days), the electrochemical reaction could be registered on the metal substrate/corrosion product interface, and the adsorption mechanism was evident in the later experimental days.

The presence of one semicircle and one time constant at all the times is shown in Figs. 4a and 4b, respectively, when the coating thickness is 0.50 mm. The impedance increases with time until 21 days. It is the opposite result from the typical water uptake impedance behavior in which the coating impedance decreases with time; this phenomenon was observed in previous work as well.[30,31] A general explanation was that the polymer structure of coating was modified during the water transport process and reflected on the EIS spectra. Subsequently, the impedance decreased at 31 and 55 days. The other remarkable feature in the results is that the impedance on the first day was one semicircle at HF and nonlinear response at LF. This latter feature is attributed to the high impedance magnitudes as a consequence of the thicker layer. This had less influence as time increased. All these experiments for 0.50 mm thickness are assumed to be in the stage I of the experimental damage evolution process.

In a general comparison of these results, the coating impedance increases as the thickness increases at pH 4. The increment–decrement of the coating impedance could be due to an inhomogeneous water distribution, a chemical reaction, and/or other factors. As a result, the coating had an atypical behavior compared to that expected by a standard coating, in which the impedance tends to decrease with time when water is absorbed by the polymeric matrix.

Transmission line modeling theory for each formed layer

Interface substrate/corrosion product porous layer modeling development

A general TLM mathematical formulation assuming a particular solution for a pore that depends on the boundary conditions of the system was proposed by Bisquert.[32] Previously, Park and Macdonald had developed a TLM cylindrical porous layer.[18] The schematic interface representation of our system is shown in Fig. 5a and is divided in each layer, outer layer illustrated in Fig. 5b, inner layer and substrate interface in Fig. 5c.

Current and voltage equations provide a dependent differential equation system that is based on Kirchhoff's and Ohm's laws and is used to quantify the impedance of a single cylindrical pore. We assume that the electrolyte resistance inside the pore and the iron oxide are constant along the pore. This latter makes it possible to find an analytical solution for the impedance of a pore that is shown in equation (1).

$$Z_\mathrm{p} = \frac{R_\mathrm{o}R_\mathrm{e}L}{R_\mathrm{o}+R_s} + \frac{2\beta^{1/2}R_\mathrm{o}R_\mathrm{e} + \gamma\beta^{1/2}(R_\mathrm{o}^2+R_\mathrm{e}^2)b + aR_\mathrm{e}^2c}{\beta^{1/2}(R_\mathrm{o}+R_\mathrm{e})(\beta^{1/2}c+ab)}.$$

(1)

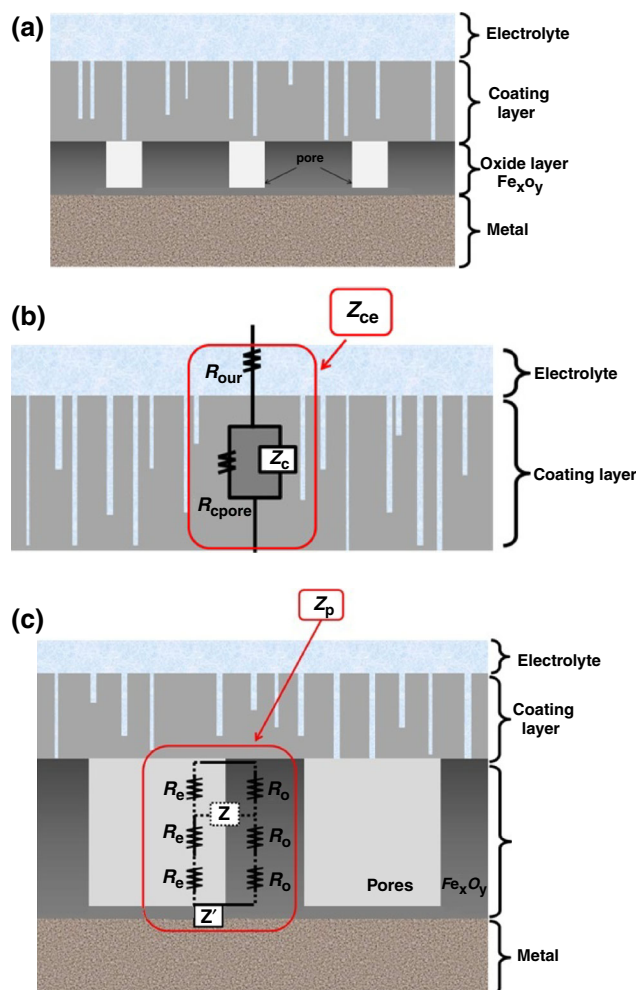Here Z_p is equal to the impedance of a single pore, where

Fig. 5: (a) Layers in the experimental system; (b) the analogy element representation for coating layer; (c) detailed description of impedance per cylindrical pore, Z_p

$$a = \frac{R_\mathrm{o}+R_\mathrm{e}}{Z'}, b = \cos h(\beta^{0.5}L), \text{ and } c = \sin h(\beta^{0.5}L),$$

$$\beta^2 = \frac{R_\mathrm{o}+R_\mathrm{e}}{Z}.$$

By assuming the porous average shape is a uniform cylinder, the following expressions for R_o, R_e, Z', and Z are represented in the following expressions:

$$R_\mathrm{o} = \frac{\rho_\mathrm{o}n}{\theta A},$$

(2)

$$R_\mathrm{e} = \frac{\rho_\mathrm{e}n}{(1-\theta)A},$$

(3)

where ρ_o is oxide resistivity, ρ_e is electrolyte resistivity, n is the number of pores, θ is the iron oxide fraction coverage on the metal surface, A is the area of the porous oxide film, R_o is the resistance of the oxide layer per pore, R_e is the resistance of the electrolyte

per pore, and L is the thickness of the iron oxide layer. The specific impedances of the pore wall and base are represented by Z_w and Z_b, respectively. The Z is the impedance of the wall per pore, and Z' is the impedance at the pore base per pore as illustrated in Fig. 5c. The Z and Z' parameters are described in equations 4 and 5, respectively

$$Z = \frac{Z_w n^{0.5}}{2\pi^{0.5}(1-\theta)^{0.5} A^{0.5}} \tag{4}$$

$$Z' = \frac{Z_b n}{(1-\theta) A}. \tag{5}$$

While the parameters R_o, R_e, Z, and Z' are parameters that are independent of length, the total impedance of the porous film by assuming all the pores in parallel is

$$Z_t = \frac{Z_p}{n}. \tag{6}$$

The specific impedance at the wall and the pore base can be represented by the following equivalent circuit expressions for pH 4 at early exposure conditions:

$$Z_w = \frac{1}{\frac{1}{R_{ow}} + Q_{ow}(j\omega)^{n_{ow}}}, \tag{7}$$

$$Z_b = \frac{1}{\frac{1}{R_b} + Q_b(j\omega)^{n_b}}, \tag{8}$$

where R_{ow} is the charge transfer resistance of the oxide wall, Q_{ow} is the pseudo-capacitance of the oxide wall, n_{ow} is the coefficient of the pseudo-capacitance element for the oxide wall, R_b is the charge transfer resistance for the pore base, Q_b is the pseudo-capacitance for the pore base, and n_b is the coefficient of the pseudo-capacitance element for the pore base. The expressions for the pore wall and base impedance for the described conditions are

$$Z = \left(\frac{n}{\Pi A(1-\theta)}\right)^{1/2} \frac{1}{\frac{1}{R_{ow}} + Q_{ow}(j\omega)^{n_{ow}}}, \tag{9}$$

$$Z' = \left(\frac{n}{A(1-\theta)}\right) \frac{1}{\frac{1}{R_b} + Q_b(j\omega)^{n_b}}. \tag{10}$$

Then, the total impedance of a porous film composed of n single dimensional pores considering the expression for the wall and base pore from expressions 9 and 10 can be calculated as

$$Z_t = \frac{1}{n}\left(\frac{R_o R_e L}{R_o + R_s} + \frac{2\beta^{1/2} R_o R_e + \gamma\beta^{1/2}(R_o^2 + R_e^2)b + aR_e^2 c}{\beta^{1/2}(R_o + R_e)(\beta^{1/2}c + ab)}\right) \tag{11}$$

Z_t considers the influence of the corrosion products/substrate interface. The total impedance of the system considering different layers (interfaces) due to the

existing mechanisms at pH 4 at longer times and within the coating layer are calculated as follows.

Adsorption mechanism at the pore base at low pH

At the pore base, we assume the adsorption reaction controlling the process is preferentially occurring at low pH. A charge balance at the interface of the oxide film and electrolyte has previously been reported.[33] We assume in our system that if v_1 is the transfer rate of metal cations (taken to be M^+) onto a monolayer surface, v_2 is the transfer rate of metal cations from the bulk to the film, v_3 and v_4 are the corresponding rates for the oxidizing species; and if an excess of cations is defined and a Taylor expansion for a perturbation in potential $\Delta E \exp(j\omega t)$ is performed, then the following expression is obtained[33]:

$$Z' = \left(\frac{n}{A(1-\theta)}\right) \frac{1}{\frac{1}{R_{inf1}} + \frac{1}{R_{zero1}}\left(\frac{h}{j\omega+h}\right) + \frac{1}{R_{inf2}}\left(\frac{j\omega}{j\omega+h}\right) + j\omega C_b}, \tag{12}$$

where R_{inf1} is the resistance for v_1 and v_2 at infinite frequency, R_{zero1} is the resistance for v_1 and v_2 at zero frequency, h is the inverse of the relaxation time, R_{inf2} is the infinite resistance for v_3 and v_4 at infinity frequency, and C_b is the capacitance on the base of the pore. It should be noted that R_{zero2} does not appear in the expression because the oxidizer is assumed to be in equilibrium with either the oxide film or the pore base interface. From these parameters, a reaction resistance can be calculated and it is used to the pore base resistance (R_b).[33] The expression of R_b is shown in equation (13).

$$R_b = \left[\frac{1}{R_{inf1}} + \frac{1}{R_{inf2}}\right]^{-1}. \tag{13}$$

For experiments performed at pH 4 after 3 days, equations (12) and (13) were used to determine the resistance at the pore base of samples with a 0.13-mm coal tar enamel coating for later exposure times ($t > 3$ days). Expression 13 standards R_b in expression 10, the total impedance Z_t as expressed in equation (11) is considered to be estimated by using expressions 12 and 13 at pH 4 and time exposure higher than 3 days.

The outer coating layer is assumed to be porous with heterogeneous distribution; the coating layer is included with the total impedance as represented in the following procedure.

Water uptake-modeling based on power law

The electric analogy describing the outer coating layer is illustrated in Fig. 5b; it is described in detail

elsewhere.[16] The assumptions for the electric analogy of the coating include: (i) the coating absorbs electrolyte to an extent that progressively decreases from the coating/electrolyte interface to the substrate/corrosion product interface; (ii) the volume fraction of the electrolyte varies along the coating thickness according to a power law, (iii) the resistivity and permeability profiles of the electrolyte-penetrated coating can be calculated through an effective medium theory corresponding to a parallel combination of the two media (electrolyte and coating material); and (iv) some pores extend from the coating/electrolyte interface to the substrate/coating interface, proving a low resistance path (see Fig. 5b).

The coating thickness is represented with δ and the dimensionless position through the coating is shown in equation (14).

$$\chi = \frac{x}{\delta}, \tag{14}$$

where x is the distance from the oxide layer/coating to the coating/electrolyte interface. The coating pore distributions are shown in Figs. 5a–5c. The majority of them have a mouth in the coating/electrolyte, but just some of them have a length equal to the coating thickness. Therefore, different planes which are parallel to the coating interfaces cross a dissimilar pore quantity. As a result at a different position, χ, the local electrolyte volume fraction, $\varphi(\chi)$, is dissimilar. The volume fraction is calculated with the power law that is shown in equation (15) (assumption ii).

$$\varphi(\chi) = \frac{\varphi(\delta)\chi^{\gamma}}{1 + \varphi(\delta)(\chi^{\gamma} - 1)}. \tag{15}$$

In this expression $\varphi(\chi)$ is dimensionless, additionally, $\varphi(0) = 0$ at $\chi = 0$ (assumption i) and $\varphi(\delta)$ at $\chi = 1$. The exponent γ and a constant phase element (CPE) exponent α are linked by the expression [16]

$$\alpha = \frac{\gamma - 1}{\gamma}. \tag{16}$$

The condition $\varphi(0) \neq 0$ is not considered because R_{cpore} takes contribution of the pores which cross from the electrolyte/coating interface to the coating/corrosion products. As a consequence, R_{cpore} is in parallel with the electrolyte-modified coating impedance, Z_c, The term Z_c is represented in equation (17)

$$Z_c = \delta \int_0^1 \frac{1}{\rho(\chi)^{-1} + j\omega\varepsilon(\chi)\varepsilon_0} d\chi. \tag{17}$$

The last equation is the result of the assumption that each element layer can be depicted by a parallel combination of resistance $\rho(\chi)d\chi$ and capacitance $\varepsilon(\chi)\varepsilon_0 d\chi$; where $\rho(\chi)$ is the resistivity of the coating

and $\varepsilon(\chi)$ is the permittivity. They are represented in equations (18) and (19), respectively

$$\rho(\chi)^{-1} = \rho_{\text{w}}^{-1}\varphi(\chi) + \rho_{\text{c}}^{-1}[1 - \varphi(\chi)], \tag{18}$$

$$\varepsilon(\chi) = \varepsilon_{\text{w}}\varphi(\chi) + \varepsilon_{\text{c}}[1 - \varphi(\chi)]. \tag{19}$$

The subscripts w and c represent the electrolyte and the coating property.

The information described above leads to the combined impedance including coating and electrolyte layer which is shown as follows as well as in Fig. 5b:

$$Z_{\text{ce}} = \left[\frac{1}{Z_c} + \frac{1}{R_{\text{cpore}}}\right]^{-1}. \tag{20}$$

Therefore, the total impedance of the electrochemical system considering the system coating/corrosion product/substrate interface as shown in Fig. 5a, is given by

$$Z_{\text{t2}} = A(R_{\text{out}} + Z_{\text{ce}} + Z_{\text{t}}), \tag{21}$$

where Z_{t2} is the total impedance of the electrolyte/coating/oxide layer/substrate system, R_{out} is the resistance of the electrolyte, Z_{t} is the corrosion products/substrate impedance, and Z_{ce} is the combined impedance of coating and electrolyte uptake.

The $(R_{\text{out}} + Z_{\text{ce}})$ expression is used when the oxide response was not detected because of a high coating thickness. As a consequence, the system was temporarily assumed to be like a coating/substrate interface where the water inhomogeneous distribution could be increasing the coating impedance. Hence, these parameters were applied in the sample with 0.50-mm coal tar thickness.

Quantitative analysis using TLM for the samples with 0.13 mm coating thickness

TLM was used to describe the impedance response of steel substrate samples covered by oxide layer as an inner layer and a 0.13-mm-thick coal tar enamel outer layer exposed to an electrolyte solution at pH 4. In order to fit the required parameters, genetic algorithm (GA) and evolutionary strategies (ES) are used following the Levenberg–Marquardt methods of solution. The calculation follows five basic steps as described previously.[34] The fitting included an optimization based on an error less than 5% for all frequencies. Figures 6a and 6b and 7a and 7b show the comparison between the fitting and the experimental results. Tables 1 and 2 summarize the evolution of the parameters used for the fitting process with time for 0.13 mm thickness and low pH conditions. Eight parameters were considered for the fitting-analysis process during stage I and transition for stage II in
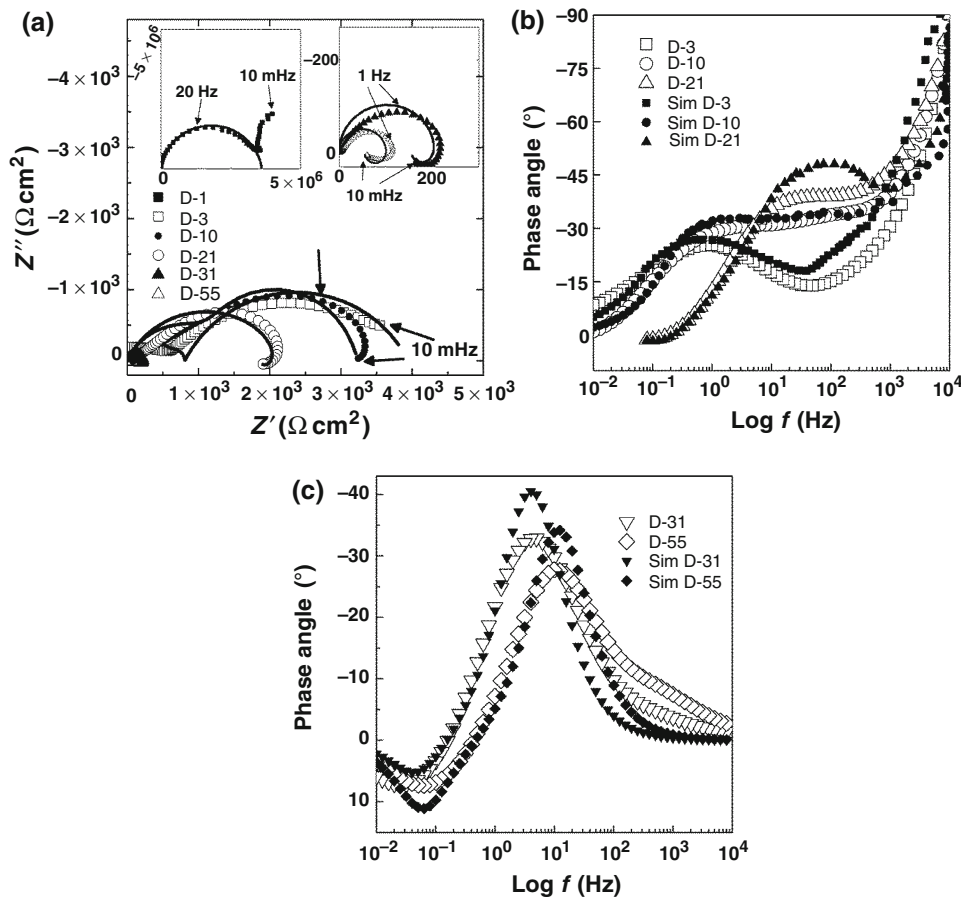
Fig. 6: (a) Nyquist diagram; (b) 1, 10, and 21 days Bode diagram; and (c) 31 and 55 days Bode diagrams of a plate coated with 0.13 mm of coal tar in NaCl solution at pH 4. The solid lines in (a) are the simulated results
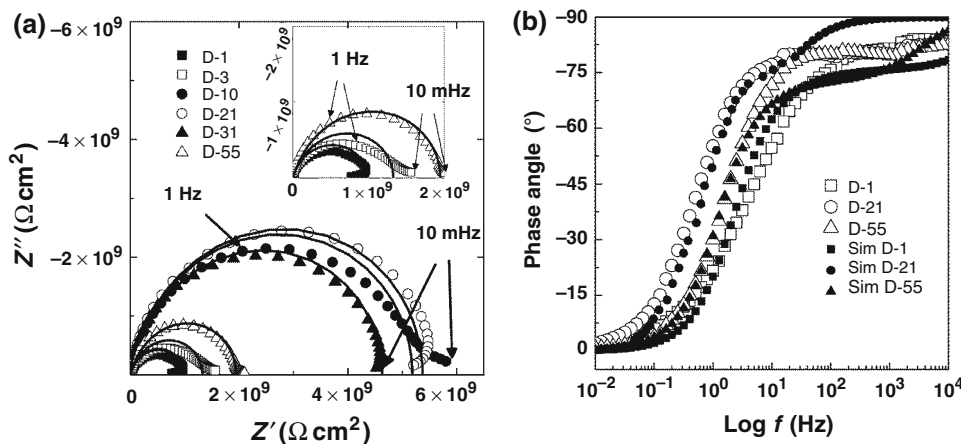

Fig. 7: (a) Nyquist diagram; (b) 1, 21, and 55 days Bode of a plate coated with 0.50 mm of coal tar in NaCl electrolyte solution at pH 4. The solid lines in (a) are the simulated results

Table 1. Ten parameters in which some were different from stage I/II were included in the analysis for the stage II/III for the damage evolution; eight of them are shown in Table 2. The constant parameters related to

the characteristics of the interface and not included in Table 2 are: the oxide resistivity (ρ_o = 5000 Ω cm) and the electrolyte resistivity (ρ_s = 50 Ω cm). The coverage factor (θ) was 0.8 for 10 days, 0.65 for 21 days, 0.5 for

Table 1: Fitting parameters for the sample with a 0.13 mm coating thickness at pH 4 for early stage

| Day	Stage	R_{ow} (Ω cm^2)	Q_{ow} (F cm^{-2} s^{n-1})	n_{ow}	R_b (Ω cm^2)	Q_b (F cm^{-2} s^{n-1})	n_b	R_{cpore} (Ω cm^2)	$\varphi(\delta)$	α
1	I	NA	NA	NA	NA	NA	NA	3.65×10^6	0.025	0.9
3	I/II	6091	8.84×10^{-4}	0.99	606	4.80×10^{-6}	0.6	250	0.9	0.8

Table 2: Fitting parameters for the sample with a 0.13-mm-thick coating at pH 4 with time

Day	Stage	R_{ow} (Ω cm^2)	Q_{ow} (F cm^{-2} s^{n-1})	n_{ow}	R_{inf1} (Ω cm^2)	R_{zero1} (Ω cm^2)	R_{inf2} (Ω cm^2)	C_b (F cm^{-2})	h (s^{-1})	R_b (Ωcm^2)
10	II	2500	2.06×10^{-3}	0.7	1062	1930	451	1.00×10^{-5}	4.26	316
21	II/III	1910	1.40×10^{-3}	0.73	1891	1047	1393	1.00×10^{-6}	1.02	202
31	III	271	9.97×10^{-5}	0.71	334	249	438	4.53×10^{-4}	0.26	189
55	III	132	1.00×10^{-4}	0.78	121	83	365	2.81×10^{-4}	0.26	91

31 days, and 0.1 for 55 days while the thickness (L) was 9 μm for 10 days, 7 μm for 21 days, 5 μm for 31 days, and 1 μm for 55 days. The coverage factor and the thickness decreased over time due to the iron oxide (Fe$_x$O$_y$) dissolution at pH 4. The remaining factors were held constant during fitting. Their values are presented: n is the total number of pores, which was constant at 1250 pores. The area, A, was fixed at the actual experimental area of 4.52 cm^2.

Figure 8 represents three stages of evolution mechanisms with time. The interface system starts at stage I on first day. As shown in Fig. 8a, the water uptake process is the dominant process at this time. The Nyquist plot in Fig. 3a indicated the water uptake in the coating is the dominant mechanism on day 1. In addition, according to Table 1, the coating pore resistance, R_{cpore}, is estimated to be 3.65×10^6 Ω cm^2 and the volume fraction of the coating ($\varphi(\delta)$) is a high value in the surface of the dry coating. Both values are an indication of a poor coating performance.[27]

At day 3, the pore coating resistance (R_{cpore}) was 250 Ω cm^2, whereas the corrosion product pore wall resistance (R_{ow}) and pore base resistance (R_b) were 6091 and 606 Ω cm^2, respectively. The coating resistance decreased due to the electrolyte content and/or the chemical degradation. The volume fraction was 0.9 in the coating surface resulting from the polymer structure was almost saturated with water. The appearance of R_{ow} and R_b indicates stage II activity, illustrated in Fig. 8b. The presence of ionic species at the porous corrosion product/substrate interface influences the dominance of the charge transfer mechanism; the cathodic reaction occurs at the pore interface, the hydrogen ion presented in the electrolyte serves as the reactant for the reduction reaction within the pore.
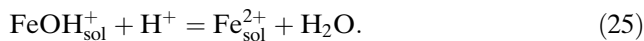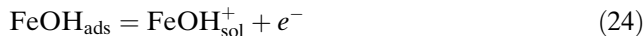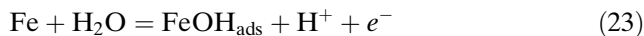
$$2H^+ + 2e^- = H_2. \tag{22}$$

(a)

(b)

(c)
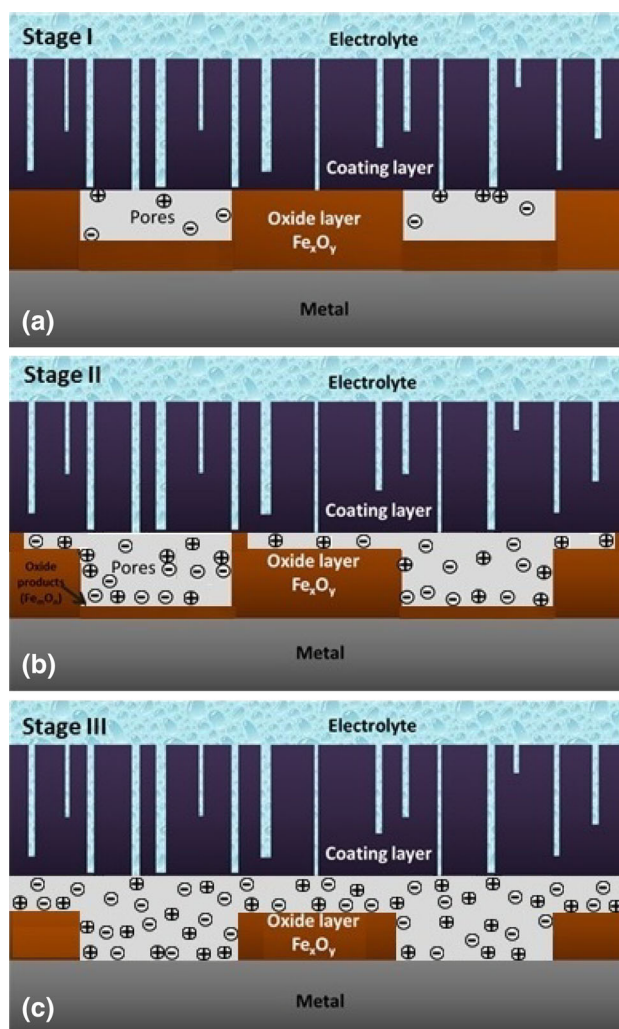
Fig. 8: Scheme of the experimental damage evolution for sample in pH 4.0 electrolyte for (a) stage I, (b) stage II, and (c) stage III

At day 3, the R_{ow} and R_b magnitudes indicate the number of potential sites available for the charge transfer reaction. The resistance of the pore wall, R_{ow}, was determined to be 6091 Ω cm^2, while the resistance of the pore base, R_b, was estimated to be 606 Ω cm^2, which is less than the wall resistance, R_{ow}. In other words, the walls of the preformed iron oxide layer (Fe_xO_y) have lower active sites for the reduction reaction than the oxide layer formed on the pore base (Fe_xO_y). Although the coating was water-saturated and partially damaged by a homogeneous reaction, the coating still prevented free contact between the electrolyte and the oxide. Meanwhile, corrosion products (Fe_xO_y) started to dissolve at the inner layer pore base due to the electrochemical dissolution of the iron oxide. The following values for pseudo-capacitances were obtained by TLM: 8.84×10^{-4} F cm^{-2} s^{n-1} for the pore wall (Q_{ow}) and 4.86×10^{-6} F cm^{-2} s^{n-1} for the pore base (Q_b). The largest magnitude for pseudo-capacitance, on the order of 0.84 mF cm^{-2} s^{n-1}, was observed for Q_{ow} from the oxide layers of samples in aqueous media.[35] The ionic species have a transport path within the porous layer semiconductor material, whereas the magnitude of the pore base, on the order of μF cm^{-2} s^{n-1}, was expected for double-layer interfaces in aqueous media.[36] This latter is attributed to the different oxide composition (Fe_xO_y)/electrolyte interface prevailing at the base pore. The R_{cpore} is 250 Ω cm^2 and the water volume fraction in the interface electrolyte/coating $\varphi(\delta)$ is 0.90. A low pore resistance and a high water volume fraction are an indication that the coating has been damaged by the electrolyte uptake and/or homogeneous reactions at low pH.

At 10 days, a semiloop at HF and medium frequencies (MF) appear in the Nyquist plot in Fig. 3a. This is attributed to the oxide layer pores influence, and the initiation of a positive capacitive loop at LF, which is associated with the presence of adsorbed species at corrosion products/substrate interface. In Table 2, the parameters were included in the analysis for the stages II and III at pH 4. Following 55 days of exposure, the electrochemical system faces the transition between stage II and III of the damage evolution as illustrated in Figs. 8b and 8c.

At day 10, the number of sites favoring the charge transfer reaction at the oxide layer increases with time. The continuous electrolyte and ionic transport within the coating reaching the pore base and wall influence the activation (charge transfer) at this location, as illustrated in Fig. 8b. The resistance of the pore base, R_b, at 10, 21, 31, and 55 days was estimated by equation (13), which is based on the resistance at "infinite" (R_{inf1} and R_{inf2}) and "zero" (R_{zero1}) frequencies. These frequencies are related to the ion charge rates derived from the metal substrate (steel) and a iron oxide monolayer.[33] The inductive loop observed in Fig. 3a at LF starting at 10 days has been associated with the excess of cations over ions in the surface corrosion product monolayer following the substrate oxide pore layer in stage II. The adsorption

of an intermediate product on the substrate surface is according to the following reactions on the metal surface or corrosion product[37]

$$Fe + H_2O = FeOH_{ads} + H^+ + e^- \qquad (23)$$

$$FeOH_{ads} = FeOH_{sol}^+ + e^- \qquad (24)$$

$$FeOH_{sol}^+ + H^+ = Fe_{sol}^{2+} + H_2O. \qquad (25)$$

The Nyquist plot, Fig. 3a, seems to show the impedance signature characteristic of inductive behavior at the later times (10 days). TLM estimated magnitudes of R_b and R_{ow} at 10 days were determined to be 316 and 2500 Ω cm^2, respectively. The R_{ow} having a higher magnitude than R_b suggests that charge transfer was more dominant at the base than the walls of the pores. The continuous transport and accumulation of ionic species within the pore resulted in a higher concentration of reactants for charge transfer and adsorption reaction, producing a decrease in the resistance magnitude with time. The cathodic reaction represented in expression (22) is assumed to be faster than the adsorption process due to the higher kinetic rate for the hydrogen reaction compared with the intermediate reaction occurring at the surface of pore base. As a consequence, reactions 23–25 are the rate control mechanism. The pseudo-capacitance of the pore wall (Q_{ow}) was higher than the double-layer capacitance (C_b) at the pore base; their values were 2.06×10^{-3} F cm^{-2} s^{n-1} and 1.00×10^{-5} F cm^{-2}, respectively. Q_{ow} increases from 8.84×10^{-4} to 2.06×10^{-3} F cm^{-2} s^{n-1} from day 3 to day 10 due to the area available for the ionic species at the wall interface. Q_{ow} is directly proportional to the area available for the charge transfer reaction; the dominant mechanism is changing from charge transfer to adsorption due to the excess of intermediate and solvated ions at the interface, the smaller area for the charge transfer mechanism and more space occupied for the adsorption reaction. The pore base capacitance (C_b) increases the magnitude due to the effect of the adsorbed species at the pore base. The transition from charge transfer control to adsorption dominance is evident from days 3 to 10, as illustrated in Fig. 3. The mass transfer mechanism and the coating response were less important (small R_{cpore} and high volume fraction) at stage II.

After 21 days, the impedance diagram (Fig. 3a) shows a loop at HF–MF and a semi-small positive loop at LF, similar to previous semi-adsorption mechanism occurring at 10 days. Bode representation in Fig. 3b shows one time constant at MF that is associated with the oxide layer dissolution and a second constant at LF related to the adsorption mechanism. The transition from charge transfer to adsorption dominant mechanism occurs at this time. The corrosion product porous layer hosts the cathodic reaction at the pore wall and the cations excess, producing the adsorption mechanisms at the pore base. Table 2 shows the fitting estimate for the resistance at the pore base R_b and pore wall R_{ow}, being 202 and

1910 Ω cm^2, respectively. Different magnitudes existed due to the dominant mechanisms, physical morphology and chemical composition of the corrosion products formed at each location. The resistance magnitude for both locations decreased from 10 to 21 days; however, the R_{ow} decreased slightly from 2500 to 1910 Ω cm^2 as well as Q_{ow} which decreased from 2.06×10^{-3} to 1.40×10^{-3} F cm^{-2} s^{n-1} from 10 to 21 days. This latter is attributed to the pore wall dissolution. The ions presented at the pore wall did not change in nature, the ions just changed in quantity, and the oxide pore wall has not been modified in its chemical composition but its thickness. The decrement in R_b from 10 to 21 days is associated with the growing area for charge transfer and adsorption reaction at the pore base. The C_b magnitude changed from 1.00×10^{-5} to 1.00×10^{-6} F cm^{-2}. This latter modification could be found in systems where bare steel experiences free aqueous corrosion[36]; in our system the process is mainly dominated for the charge transfer process influenced by reaction 23–25 and its adsorption mechanisms at the pore base.

The Nyquist representations (Figs. 3a and 4a) for 31 and 55 days have a smaller loop at HF–MF and a semicircle at positive capacitance at LF, which indicates that the dominant process is the adsorption of intermediate or solvated ionic species at the interface of the corrosion product/substrate. Likewise, the Bode plots in Figs. 6b and 7b show good agreement between theoretical and experimental results. One time constant at MF was obtained, and a positive angle behavior at LF was observed; this latter is related to an adsorption–desorption chemical intermediate mechanism.

At 31 and 55 days, R_{ow} decreased with time, which is explained by the change associated with the oxide area. The decrement of this latter parameter suggests that the iron oxide layer was exposed at the coating/corrosion product interface and became less dense over time, as represented in Fig. 8c. Additionally, more active sites exist at the wall location.

After 31 days, R_b and R_{ow} were determined to be 189 and 271 Ω cm^2, and Q_{ow} and C_b were determined to be 9.97×10^{-5} F cm^{-2} s^{n-1} and 4.53×10^{-4} F cm^{-2}, respectively. The following estimations were collected for the experiment at 55 days: $R_{ow} = 132$ Ω cm^2, $R_b = 91$ Ω cm^2, $Q_{ow} = 1.00 \times 10^{-4}$ F cm^{-2} s^{n-1}, and $C_b = 2.81 \times 10^{-4}$ F cm^{-2}. The results show the system is facing stage III, R_b and R_{ow} are in the same order of magnitude at 31 and 55 days. This latter could be attributed to the pore wall condition being similar to the pore base. The oxide layer has been almost dissolved. This suggests that the overall surface (base and wall pore) was dominated by the charge transfer mechanism and adsorption mechanism. The value of the relaxation time h was constant for 31 and 55 days, an indication that the excess of cations in the form of the $FeOH_{ads}^{+}$ has reached an important critical number for the adsorption mechanism. However, this resis-

tance is lower compared with the ones obtained when the oxide layers had more presence on the substrate.

Quantitative analysis for the samples with 0.50 mm coating thicknesses

The ($R_{out} + Z_{ce}$) expression, which describes the inhomogeneity of the water uptake within the coating (stage I and Fig. 8a representation), was used to fit the results of the samples with a 0.50 mm coating thickness at pH 4. The coating inhomogeneity is described through the resistivity of the water and the coating, as well as their permittivity as represented by equations 18 and 19. The constant parameters used for the calculations were: water resistivity, ρ_w, 50 Ω cm; the coating resistivity, ρ_c, 1×10^{11} Ω cm, whereas water permittivity, ε_w, was 82; and the coating permittivity, ε_c, was 8. The vacuum permittivity, ε_0, was taken to be 8.85×10^{-14} F cm^{-1} and the coating thicknesses, δ, were 0.13 and 0.50 mm. The important parameters that were needed for the fitting process were the coating pore resistance (R_{cpore}), the water fraction volume at the interface coating/electrolyte ($\varphi(\delta)$), and the variable γ (a dimensionless parameter) that is used in the calculation of the water volume fraction ($\varphi(\chi)$), which related with the CPE coefficient, α, with the water volume fraction, $\varphi(\chi)$, equation (16). These parameters are shown in Table 2 for 0.50 mm. These three parameters show a change in the profile of resistivity and permittivity in the coatings, resulting from a water distribution and/or a coating modification by chemical reaction.

The Nyquist plot and phase angle plot of the sample with a 0.5 mm thickness are shown in Figs. 4a and 4b, respectively. In the Nyquist plot, a semicircle can be observed, while in the Bode format, only one time constant is obtained. These results are related to the water uptake or stage I of the damage evolution response due to a resistance increment. The experimental results show good agreement with theoretical simulation as demonstrated in Figs. 7a and 7b.

The results for the sample with 0.50 mm coating thickness at pH 4 are shown in Table 3. R_{cpore} increased from 2.00×10^9 Ω cm^2 for day 1 to 9.00×10^{10} Ω cm^2 for 21 days while the volume fraction at the surface of the coating ($\varphi(\delta)$) decreased from 1.00×10^{-5} to 7.00×10^{-9} in the same period of time.

These latter results do not follow the traditional behavior in which the coating resistance is decreasing as the water uptake follows the process. In contrast, R_{cpore} and $\varphi(\delta)$ values could show the coating follows an inhomogeneous water distribution and/or a chemical transformation. As time increases, both R_{cpore} and $\varphi(\delta)$ reduce their value during 55 days of testing; this could be indicative of the coating water saturation and/or a chemical transformation. Tables 1 and 3 display the parameter α that is related in equation (16) with the exponent γ which describes the power law of the water volume fraction (equation 15) in each position

Table 3: Fitting parameters for the sample with 0.5 mm coating thickness at pH 4

Parameter	Stage	1-day	3-day	10-day	21-day	31-day	55-day
R_{cpore} (Ω cm^2)	I	2.00×10^9	6.10×10^9	5.60×10^{10}	9.00×10^{10}	3.00×10^{10}	2.00×10^{10}
$\varphi(\delta)$	I	1.00×10^{-5}	2.50×10^{-6}	7.00×10^{-9}	7.00×10^{-9}	9.00×10^{-9}	9.00×10^{-7}
α	I	0.84	0.80	0.82	0.82	0.82	0.805

from the electrolyte/coating to the coating/oxide layer. The α values are around 0.8 for the fittings where the model assumptions could be applied. This is in agreement with previous work[16] where this parameter value was associated with an inhomogeneous water distribution for anticorrosion coatings.

The results of both R_{cpore} and $\varphi(\delta)$ described before can be explained by the following assumptions:

(i) For the thinnest coating (0.13 mm), the water penetrates only in the direction from the coating/electrolyte interface to the coating/substrate boundary, and a homogeneous water distribution can be obtained which can be associated with a decrement in the coating resistance. To the contrary, for the thicker coating (0.5 mm), we can assume that the water penetrates not only the thickness dimension of the coating but also in a direction perpendicular to the substrate/coating interface. Hence, an inhomogeneous water distribution could be obtained in thicker coatings; this process can be supported by the coating resistance changes. This latter situation is not taken totally in the model applied to this work, but also the formulation which was done by using the Amand et al.[16] approach, where they considered as the main assumption the water flow is uni-dimensional.

(ii) The pH conditions was selected to accelerate the damage of the coating, although the results showed the R_{cpore} and $\varphi(\delta)$ increased in the first instance. We believe an additional factor that could contribute in the increment is a chemical transformation that could change the coating resistivity in the coating outer layers.

Conclusions

Three stages of the damage evolution concept are identified and associated as a result of experimental conditions. The damage evolution for the coating/oxide/steel sample at pH 4 and thinnest coating layer (0.13 mm) produced three stages characterized by interfacial mechanisms: the mass transport as stage I, charge–mass transport mix as stage II, and finally the active-adsorption mechanisms associated with stage III.

The sample with 0.50 mm thickness produced one stage for the damage evolution process; the mechanism included water uptake. Meanwhile, a distinct increase in coating resistance was observed for this thickness during the first stage of damage evolution. This abnormal behavior might occur because of several reasons, such as an inhomogeneous distribution of water parallel and perpendicular to the coating, or a chemical reaction between the coating and the environment, among others.

TLM could characterize and described the pores' influence for each dominant mechanism prevailing at each defined stage; the pores of the preformed corrosion product influenced the mechanisms due to the pores geometry and distribution. TLM coupled with EIS modeling could assess quantitatively the coating/corrosion product/substrate evolution by association of defined parameters with the mechanisms proposed in each stage.

References

1. Akbarinezhad, E, Bahremandi, M, Faridi, H, Rezaei, F, "Another Approach for Ranking and Evaluating Organic Paint Coatings Via Electrochemical Impedance Spectroscopy." *Corros. Sci.*, **51** (2) 356–363 (2009)
2. Wicks, ZW, Jones, FN, *Organic Coatings: Science and Technology*. Wiley Interscience, Hoboken, 1999
3. Baukh, V, *Water Transport in Multilayer Coating*. Eindhoven University, Eindhoven, 2012
4. Li, C, Cao, B, Wu, Y, "An Electrochemical Method for Evaluating the Resistance to Disbondement of Anticorrosion Coatings on Buried." *J. Univ. Sci. Technol.*, **14** 414 (2007)
5. Xu, J, Wang, K, Sun, C, Wang, F, Li, X, Yang, J, Yu, C, "The Effects of Sulfate Reducing Bacteria on Corrosion of Carbon Steel Q235 Under Simulated Disbonded Coating by Using Electrochemical Impedance Spectroscopy." *Corros. Sci.*, **53** (4) 1554–1562 (2011)
6. Reynolds, G, Barrett, Z, Williams, G, "An Investigation of the Influence of Physical Vapour Deposited Aluminium Layers on the Kinetics of Organic Coating Disbondement on Iron." *Corros. Sci.*, **70** 82–92 (2013)
7. Xia, D, Song, S, Wang, J, "Fast Evaluation of Degradation Degree of Organic Coatings by Analyzing Electrochemical Impedance Spectroscopy Data." *Trans. Tianjin Univ.*, **18** 15–20 (2012)
8. Mansfeld, F, Han, L, Lee, C, Zhang, G, "Evaluation of Corrosion Protection by Polymer Coatings Using Electrochemical Impedance Spectroscopy and Noise Analysis." *Electrochim. Acta*, **43** 1933–2945 (1998)

9. Bierwagen, G, Kerry, A, Hinderliter, B, "Ion Liquid Enhanced Electrochemical Characterization of Organic Coatings." *Prog. Org. Coat.*, **63** 250–259 (2008)

10. Hinderliter, B, Croll, S, Tallman, D, "Interpretation of EIS Data from Accelerated Exposure of Coated Metals Based on Modeling of Coating Physical Properties." *Electrochim. Acta*, **51** 4505–4515 (2006)

11. Mansfeld, F, "Use of Electrochemical Impedance Spectroscopy for the Study of Corrosion Protection by Polymer Coatings." *J. Appl. Electrochem.*, **25** (3) 187–202 (1995)

12. Deflorian, F, Fedrizzi, L, Bonora, PL, "Impedance Study of the Corrosion Protection Properties of Fluoropolymer Coatings." *Prog. Org. Coat.*, **23** (1) 73–88 (1993)

13. Akbarinezhad, E, Rezaei, F, Neshati, J, "Evaluation of a High Resistance Paint Coating with EIS Measurements: Effect of High AC Perturbations." *Prog. Org. Coat.*, **61** (1) 45–52 (2008)

14. Walter, G, "The Application of Impedance Methods to Study the Effects of Water Uptake and Chloride Ion Concentration on the Degradation of Paint Films—II. Free Films and Attached/Free Film Comparisons." *Corros. Sci.*, **32** (10) 1085–1103 (1991)

15. Haruyama, S, Asari, M, Tsuru, T, *Corrosion Protection by Organic Coatings*. Proceedings of the Electrochemical Society, Pennington, NJ, 1987

16. Amand, S, Musiani, M, Orazem, M, Pébère, N, Tribollet, B, Vivier, V, "Constant-Phase-Element Behavior Caused by Inhomogeneous water Uptake in Anti-corrosion Coatings." *Electrochim. Acta*, **87** 693–700 (2013)

17. Liu, Y, Wang, J, Liu, L, Li, Y, Wang, F, "Study of the Failure Mechanism of an Epoxy Coating System Under High Hydrostatic Pressure." *Corros. Sci.*, **74** 59–70 (2013)

18. Park, J, Macdonald, D, "Impedance Studies of the Growth of Porous Magnetite Films on Carbon Steel in High Temperature Aqueous Systems." *Corros. Sci.*, **23** (4) 295–315 (1983)

19. Raistrick, ID, "Impedance Studies of Porous Electrodes." *Electrochim. Acta*, **35** (10) 1579–1586 (1990)

20. Floyd, M, "An Examination of Oxidative Passivated Surfaces on 19th Century Colt Revolver Barrels." Scripps Senior Theses, Paper 120 (2012)

21. Allahar, K, Battocchi, D, Bierwagen, G, Tallman, D, "Transmission Line Modeling of EIS Data for a Mg-Rich Primer on AA 2024-T3." *J. Eletrochem. Soc.*, **157** (3) C95–C101 (2010)

22. Allahar, K, Battochi, D, Orazem, ME, "Modeling of Electrochemical Impedance Data of a Magnesium-Rich Primer." *J. Eletrochem. Soc.*, **155** (10) E143–E149 (2008)

23. Cornell, S, "Bluing and Browning Steel Articules." *Chem. Metall. Eng.*, **24** (7) 301–304 (1921)

24. Kato, CP, Pickering, HW, "A Rotating Disk Study of the Corrosion Behavior of Cu–9.4Ni–1.7Fe Alloy in Air-Saturated Aqueous NaCl Solution." *J. Eletrochem. Soc.*, **131** (6) 1219–1224 (1980)

25. Moraes, SR, Huerta-Vilca, D, Motheo, AJ, "Corrosion Protection of Stainless Steel by Polyaniline Electrosynthesized from Phosphate Buffer Solutions." *Prog. Org. Coat.*, **48** (1) 28–33 (2003)

26. Pourbaix, M, *Atlas of Electrochemical Equilibria in Aqueous Solutions*. National Association of Corrosion Engineers, Houston, 1974

27. Cornell, M, Rochelle, U, *Iron Oxides:Structure, Properties, Reactions, Ocurrences and Uses*. Willey-VCH, Hoboken, NJ, 2007

28. Huang, Y, Shih, H, Daugherty, J, Mansfeld, F, "Evaluation of the Properties of Anodized Aluminum 6061 Subjected to Thermal Cycling Treatment Using Electrochemical Impedance Spectroscopy (EIS)." *Corros. Sci.*, **51** (10) 2493–2501 (2009)

29. Conde, A, de Damborenea, J, "Electrochemical Impedance Spectroscopy for Studying the Degradation of Enamel Coatings." *Corros. Sci.*, **44** (7) 1555–1567 (2002)

30. Amirudin, A, Thieny, D, "Application of Electrochemical Impedance Spectroscopy to Study the Degradation of Polymer-Coated Metals." *Prog. Org. Coat.*, **26** (1) 1–28 (1995)

31. Liu, C, Bi, Q, Matthews, A, "EIS Comparison on Corrosion Performance of PVD TiN and CrN Coated Mild Steel in 0.5 N NaCl Aqueous Solution." *Corros. Sci.*, **43** 1953–1961 (2001)

32. Bisquert, J, "Influence of the Boundaries in the Impedance of Porous Film Electrodes." *Phys. Chem. Chem. Phys.*, **2** (18) 4185–4192 (2000)

33. Armstrong, R, Edmondson, K, "The Impedance of Metals in the Passive and Transpassive Regions." *Electrochim. Acta*, **18** (12) 937–943 (1973)

34. Rosas, O, Saunders, J, Castaneda, H, "Interfacial Electrochemical Analysis on LoCoO$_2$/Carbon Nanotubes Layers as Cathode Active Composite in Aqueous Electrolytes." *Electrochim. Acta*, **113** 77–86 (2013)

35. Kármán, F, Felhösi, I, Kálman, E, Cserny, I, Kövér, L, "The Role of Oxide Layer Formation During Corrosion Inhibition of Mild Steel in Neutral Aqueous Media." *Electrochim. Acta*, **43** (1–2) 69–75 (1998)

36. Mouanga, M, Puiggali, M, Devos, O, "EIS and LEIS Investigation of Aging Low Carbon Steel with Zn–Ni Coating." *Electrochim. Acta*, **106** 82–90 (2013)

37. Burstein, G, Davis, D, "The Effect of Bicarbonate on the Corrosion and Passivation of Iron." *Corrosion*, **36** 416–422 (1980)